Nonlinear control of a grid connected hybrid energetic systems (HES) based on photovoltaic-fuel cells distributed power generation systems

Said Khoudiri [1]✉, Fateh Benchabane[1], Khaled Yahia[3]

1 Electrical Engineering Department, University of Djelfa, B.P. 3117 R.P. 17000, Djelfa, Algeria

2 Laboratoire de Modélisation des Systèmes Energétiques, LMSE. B.P. 145 R.P. 07000, Biskra, Algérie

3 Laboratoire de Génie Energétique et Matériaux, LGEM. B.P. 145 R.P. 07000, Biskra, Algérie

Received 1 May 2017
Published online: 24 May 2018

Keywords
Hybrid Energetic Systems (HES)
Solid Oxide Fuel Cell (SOFC)
Photovoltaic (PV)
Sliding Mode Control
Maximum Power Point Tracking
Grid power management

Abstract: This paper presents a discrete-time integral sliding mode control for a grid connected hybrid energetic systems (HES) based on photovoltaic-Solid oxide fuel cell (SOFC) for distributed power generation systems. The proposed HES systems employ solid oxide fuel cell (SOFC) and photovoltaic panels as main sources, supercapacitors as complementary sources, and controlled DC-DC boost converter and three levels NPC inverter. A maximum power point tracking (MPPT) control is used in order to maximize the power of the photovoltaic system. The proposed control consists of a power management grid interface inverter transferring the energy from the hybrid sources into the grid by controlling the main utility grid and the common DC voltage active and reactive power. The obtained simulation results show the effectiveness and robustness of the proposed control strategy. Keywords: Hybrid Energetic Systems (HES), Solid Oxide Fuel Cell (SOFC), Photovoltaic (PV), Sliding Mode Control, Maximum Power Point Tracking (MPPT), Grid power management.

1. Introduction

Recently distributed energy sources, such as fuel cells (FC), and photovoltaic (PV) cells are increasingly being used (Paolo and Lasseter 2006; Lasseter 2011).They have been initially used in stand-alone applications, then as a part of hybrid energy systems. This hybrid energetic system (HES) is now growing due to the need to provide continuous, clean, and reliable supply of electricity (Lopes et al. 2006). The fuel cell such as SOFC is a good alternative source. It keeps generating DC power as long as the fuel (hydrogen and oxygen) is available, with a better efficiency (about 60%) compared to regular batteries. Hence, by changing the FC output power, the hybrid source output becomes controllable (Larminie and Dicks 2003).

In the grid-connected mode, the hybrid source is connected to the main grid at the Point of Common Coupling (PCC) and deliver power using DC/AC interface inverter. When the load demands changes, the power supplied by the hybrid system as well as the power delivered by the main grid must be properly adjusted to meet load demand. For control purposes, it is necessary to study the whole system with considering the dynamical and physical properties of each power sources. Different strategies based on operating modes and combining technical-economic aspects are considered for the power management (Khanh et al. 2010). In general PV-FC hybrid source has two control modes (Khanh et al. 2010): the Unit-Power Control (UPC) mode and the Feeder-Flow Control (FFC) mode. In the UPC mode, the hybrid system output power is regulated to be independent of the load demand. This output is fixed according to its components maximum power capability and can be regulated at any time to ensure the main grid requirements. If there is a rise of the local load, this variation will be compensated by the main grid. In the FFC mode, the feeder flow is regulated to a constant. The extra load demand is picked up by the hybrid source, and, hence, the feeder reference power must be known. In this work, the two modes will be considered, the fuel cell acts as a secondary source to ensure a stable and constant power delivered to the load and main grid also as back up during low PV output.

The main objective of this paper is to propose a constant frequency sliding mode controller which allow a reliable power sharing between power sources in each operating mode (Hazem et al. 2014). The main challenge is the control of the shared active and reactive power output and the control of system voltage quality (low THD with fixed frequency) and DC bus voltage value. Therefore, the choice of the controller plays a vital role in proper and safety operation of PV-FC grid system. The proposed hybrid energetic system (HES) configuration and the power management strategy must actively distribute the power demand among the main and auxiliary power sources even for the case of unbalanced load conditions.

2. Modeling description and controller design

The adopted hybrid energetic system uses the FC and PV units as the main power sources shown in figure 1. This distributed

✉ Corresponding author. E-mail address: khoudiri1said@gmail.com

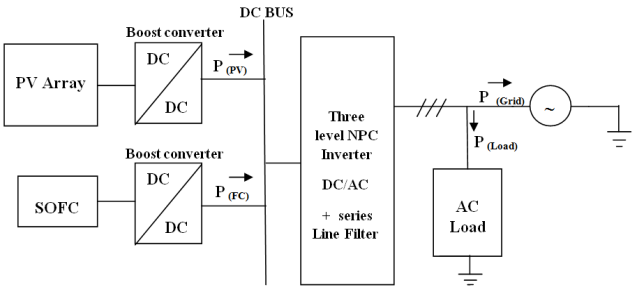

Fig.1. System overview of the PV/FC hybrid energetic system

generation units are connected to the grid through two DC/ DC boost converters, then a three level NPC VSI interface module with a series line inductor as a filter to reduce the generated harmonics. The DC side voltage of the VSI is kept constant by the appropriate control of each boost converter. The HES controller is designed for FC and PV converters fulfill the DC link power demand and the supercapacitors converter regulates the DC link voltage. The real and reactive powers are decoupled into reference currents in (d-q) axis in 'reference current calculation' block, and then controlled by the proposed 'sliding mode controller' in order to generate the appropriate reference voltages to control the three level inverter. This last step is done using a three level space vector modulation. Phase Lock Loop (PLL) is used to synchronize frequency and phase of the system with the main grid.

2.1. Photovoltaic (PV) array model

The mathematical relationship for the current and voltage in the single-diode equivalent circuit of PV can be described as:

$$I = I_{ph} - I_S \times \left[e^{\frac{q\,(V+I\times R_S)}{A\times K\times T}} - 1\right] - \frac{V+I\times R_S}{R_{Sh}} \quad (1)$$

$$I = N_P\, I_{ph} - N_P \times I_s \times \left[exp\left(\frac{q}{A\times K\times T}\left(\frac{V}{N_S} + \frac{I\times R_S}{N_P}\right)\right) - 1\right] - \frac{N_P}{R_{sh}}\left(\frac{V}{N_S} + \frac{I\times R_S}{N_P}\right) \quad (2)$$

Where: I_{ph} is photo current source; I_S : is diode saturation current; q : is electron charge (1.602 × 10-19 C); K : is Boltzmann constant (1.381 × 10-23); T : is cell temperature; A : is PN junction ideality factor; *Ns*, *Np*: are respectively cell numbers of the series and parallel cells; *Rs* : the internal losses and shunt resistance; R_{sh} in parallel with diode to take into account leakage current to the ground (Villalva et al. 2009).

Photo current is the function of solar radiation and cell temperature described as :

$$\mathrm{I_{ph}} = \left(\frac{S}{S_{ref}}\right) \times \left[I_{ph,ref} + C_T\left(T - T_{ref}\right)\right] \quad (3)$$

Where : S is the real solar radiation (W/m2); *Sref*,*Tref* : are respectively the solar radiation, cell absolute temperature, photo current in standard test conditions; C_T : is the temperature coefficient (*A*/ *K*). The diode saturation current Is varies with the cell temperature as:

$$\mathrm{I_S} = \mathrm{I_{S,ref}} \times \left(\frac{\mathrm{T}}{\mathrm{T_{ref}}}\right)^3 \times \exp\left[\frac{\mathrm{q\times E_g}}{\mathrm{A\times K}} \times \left(\frac{1}{\mathrm{T_{ref}}} - \frac{1}{\mathrm{T}}\right)\right] \quad (4)$$

Where : *Is,ref* is the diode saturation current in standard test conditions; *Eg* : is the band-gap of the cell semi-conductor (*ev*) depending on the cell material.

2.2. Solid oxide fuel cell (SOFC) modeling

Solid oxide fuel cells (SOFCs) work at very high temperatures (around 800°C to 1,000°C). They can have efficiencies of over 60% when converting fuel to electricity .Compared to other fuel cells, SOFCs are used extensively in large and small stationary power generation.

In order to give a model of the fuel cell stack that can describe the slow dynamics associated with the gas flows and the fuel processor operation (Bieberle and Gauckler 2002), some following assumptions need to be considered:

-The fuel cell temperature is assumed to be constant.

-The fuel cell gasses are ideal (Nernst's equation applicable).

By Nernst's equation DC voltage V_{fc} across stack of the fuel cell at current *I*, is given by the following equation :

$$V_{fc} = N_0 \times \left[E_0 + \frac{RT}{2F}\ln\left(\frac{P_{H_2}PO_2^{0.5}}{PH_2O}\right)\right] - r\, I_{fc} \quad (5)$$

Where : *Vfc* is operating DC voltage (*V*) ; E_0 : standard reversible cell potential (*V*) ; *Pi* : partial pressure of species (*Pa*) (i: hydrogen, oxygen) ; *r* : internal resistance of stack (Ω); I_{fc}: stack current (A) ; N_0: number of cells in stack; *R* :universal gas constant (*R*=8.314 *J/mol K*); *T* : stack temperature (*K*); F : Faraday's constant (*C/mol*).

The main equations describing the slow dynamics of an SOFC can be written as follows:

$$P_{ref} = V_{fc} \times I_{ref} \quad (6)$$

$$\frac{d\,I_{fc}}{dt} = \frac{1}{T_e}\left[-I_{fc} + I_{ref}\right] \quad (7)$$

$$\frac{d\,q_{H_2}^{in}}{dt} = \frac{1}{T_f}\left[-q_{H_2}^{in} + \frac{2K_r}{U_{opt}} I_{fc}\right] \quad (8)$$

$$\frac{d\,P_{H_2}}{dt} = \frac{1}{\tau_{H_2}}\left[-P_{H_2} + \frac{1}{K_{H_2}}\left[\,q_{H2}^{in} - 2\,K_r I_{fc}\right]\right] \quad (9)$$

$$\frac{d\,P_{O_2}}{dt} = \frac{1}{\tau_{O_2}}\left[-P_{O_2} + \frac{1}{K_{O_2}}\left[\frac{1}{r_{HO}}\,q_{H2}^{in} - 2\,K_r I_{fc}\right]\right] \quad (10)$$

$$\frac{d\,P_{H_2O}}{dt} = \frac{1}{\tau_{H_2O}}\left[-P_{H_2O} + \frac{2K_r}{K_{H_2O}} I_{fc}\right] \quad (11)$$

With : q_{H2} : Fuel flow (Mol/s) ; q_{O2} : Oxygen flow (*Mol/s*) ;K_{H2} : Valve molar constant for hydrogen (*Kmol/s atm*); K_{O2} : Valve molar constant for Oxygen (*Kmol/s atm*); K_{H2O} : Valve molar constant for Water (Kmol/s atm); τ_{H2} : Response time for hydrogen (*s*) ; τ_{O2} : Response time for Oxygen (*s*) ; τ_{H2O} : Response time for water (*s*) ; U_{opt} : Optimum fuel utilization ; r_{HO} : Ratio of hydrogen to oxygen ; K_r : Constant (*Kmol/s.A*); P_{ref} : Reference power (*Kw*).

2.3. DC- DC Boost converter modeling

Two boost converters are used in the studied PV-FC hybrid energetic system, and each one is controlled taking into account

the source specification. The boost converter block represented in figure 2, For the case of PV source, is used to extract the maximum power using MPPT algorithm. For the SOFC source, the boost converter is used in order to obtain the necessary fixed DC voltage using a simple PI controller (Erickson and Maksimovic 2001).

The averaged state space model of the converter is given by:

$$\dot{X}(t) = A\,X(t) + B\,V_s \tag{12}$$

Where : $X(t) = [i_L\, V_c]^T$ is the state vector, *A* and *B* : are the system matrices:

$$A = \begin{bmatrix} -\frac{1}{C(R+r_C)} & \frac{R}{C(R+r_C)}(1-D) \\ -\frac{R}{L(R+r_C)}(1-D) & -\frac{1}{L}(r_L + \frac{R\,r_C}{R+r_C}) \end{bmatrix}, B = \begin{bmatrix} 0 \\ \frac{1}{L} \end{bmatrix} \tag{13}$$

Where : r_L and r_c : are the internal series resistors (E_{sr}) of the inductor and capacitor, *D* : is the switching duty-ratio.

2.4. Maximum power point tracking (MPPT) control method

Many MPPT algorithms have been proposed in the literature (Villalva et al. 2009). The incremental conductance algorithm (ICMPPT) shown in figure 3 is more used because it is simple and has good performance under rapidly changing atmospheric conditions compared to the P&O algorithm.

2.5. Three level NPC inverter modeling and control

The idea of using multilevel inverter in the proposed HES is to reduce the size of the necessary output filter in order to reduce high-order harmonics introduced by the PWM modulation, for that reason we chose simplified equivalent circuit of the three levels NPC inverter. The most popular structure proposed as a transformer-less voltage source inverter is the diode clamped converter based on the neutral point clamped (NPC) converter proposed by Nabae. A (Erickson and Maksimovic 2001). They are more attractive for medium and high voltage applications (such as reactive power compensation, active power filters). It has the advantages that the blocking voltage of each switching device is one half of dc link voltage and the harmonics contents output voltages are far less than those of a two-level inverter at the same switching frequency (Sezen and Özdemir 2013; Benghanem and Drao 2006; Zhang et al. 2013).

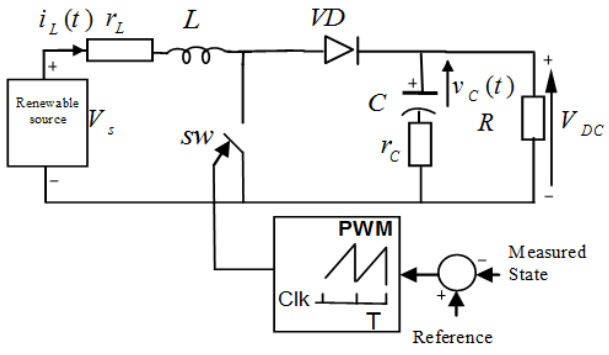

Fig. 2. Boost converter circuit block representation.

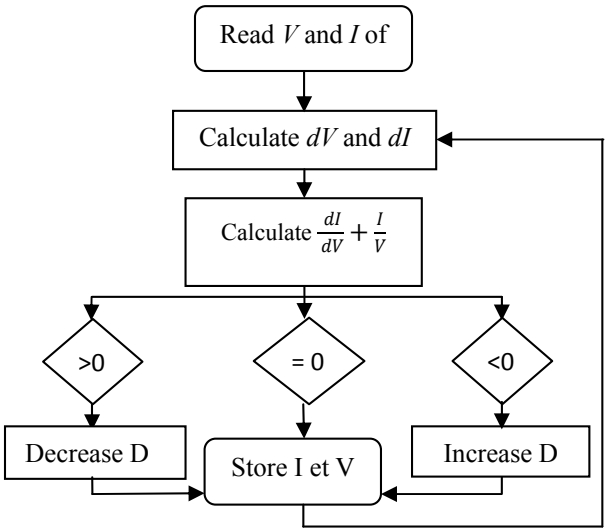

Fig. 3. Flow chart of incremental conductance (ICMPPT) method

The model of the NPC-VSI is carried out under the following assumptions:

- The power switches are ideal.

- All circuit elements are LTI (Linear Time Invariant).

- The AC voltage is a balanced three-phase system.

In the AC side using matrix form, the mathematical model is given by (Portillo et al. 2013; Bouafia et al. 2014):

$$\frac{d}{dt}\begin{bmatrix} i_a \\ i_b \\ i_c \end{bmatrix} = \begin{bmatrix} \frac{-R}{L} & 0 & 0 \\ 0 & \frac{-R}{L} & 0 \\ 0 & 0 & \frac{-R}{L} \end{bmatrix}\begin{bmatrix} i_a \\ i_b \\ i_c \end{bmatrix} + \frac{1}{L}\begin{bmatrix} V_{ga} - e_a \\ V_{gb} - e_b \\ V_{gc} - e_c \end{bmatrix} \tag{14}$$

Where the filter inductance and its internal resistance are considered *L* and *R*, and Vgi (*i*=*a*, *b*, *c*) are respectively the main grid AC voltage, and the inverter voltage .

In the DC side currents are given by : $I_{c0} = I_{c1} + I_{c2}$

Also in the DC side capacitor voltages are given by :

$$\frac{d}{dt}\begin{bmatrix} U_{C1} \\ U_{C2} \end{bmatrix} = \frac{d}{dt}\begin{bmatrix} I_{C1} \\ I_{C2} \end{bmatrix}$$

Thus, in a balanced condition we can put : $U_{C1} = U_{C2} = U_C$; $I_{C1} = I_{C2} = I_C$

Finally, the output active and reactive power of the three level inverter can be given by:

$$\begin{aligned} P_g &= V_{ga} \times i_{ga} + V_{gb} \times i_{gb} + V_{gc} \times i_{gc} \\ Q_g &= \frac{1}{\sqrt{3}} \times \left(V_{gab} \times i_{gc} + V_{gbc} \times i_{ga} + V_{gca} \times i_{gb}\right) \end{aligned} \tag{15}$$

Where: V_{ga},V_{gb}, V_{gc} : are three-phase voltages at the AC bus, i_{ga}, i_{gb}, i_{gc}: are three-phase currents injected into the AC grid.

2.5.1. Model of the three level inverter in the (*dq*) frame

As part of the control strategy, the Park transformation is used to transfer coordinates from the three-phase stationary system (*a*-*b*-*c*) to the *dq* rotating coordinate system which rotates with ω

frequency using information from a three phase PLL and this is illustrated in figure 4. The transformation matrix K_s is given by:

$$K_s = \frac{2}{3}\begin{bmatrix} \cos\omega t & \cos(\omega t - 120) & \cos(\omega t + 120) \\ \sin\omega t & \sin(\omega t - 120) & \sin(\omega t + 120) \\ 1/2 & 1/2 & 1/2 \end{bmatrix} \quad (16)$$

Applying Park transformation, the state space model of the three level NPC inverter in (*dq*) frame become:

$$\frac{d}{dt}\begin{bmatrix} i_d \\ i_q \\ V_{dc} \end{bmatrix} = \begin{bmatrix} \frac{-R}{L} & \omega & 0 \\ -\omega & \frac{-R}{L} & 0 \\ 0 & 0 & 0 \end{bmatrix}\begin{bmatrix} i_d \\ i_q \\ V_{dC} \end{bmatrix} + \begin{bmatrix} \frac{1}{L} & 0 & 0 \\ 0 & \frac{1}{L} & 0 \\ 0 & 0 & \frac{1}{C_{eq}} \end{bmatrix}\begin{bmatrix} V_d \\ V_q \\ I_{dC} \end{bmatrix} + \begin{bmatrix} \frac{-1}{L}V_{gd} \\ \frac{-1}{L}V_{gq} \\ 0 \end{bmatrix} \quad (17)$$

Where :V_{gd},V_{gq} are the(*dq*) axis components of the main grid voltages, i_d and i_q : are that of the line currents, V_d and V_q : are that of the converter output voltages. C_{eq}=*C*/2 is the DC-link equivalent capacitor. V_{dc} : is the DC bus voltage and i_{dc} is equivalent DC current .

Where the dynamic DC equivalent voltage V_{dc} is: $C_{eq}\frac{dV_{dc}}{dt} = I_{dc}$

In this case, the instantaneous active and reactive power which are delivered to the grid line in (*dq*) rotating frame are given by:

$$P_s(t) = \frac{3}{2}\left(V_{sd}(t)i_d(t) + V_{sq}(t)i_q(t)\right) \quad (18)$$

$$Q_s(t) = \frac{3}{2}\left(-V_{sd}(t)i_q(t) + V_{sq}(t)i_d(t)\right) \quad (19)$$

In the reference frame synchronized with the grid voltage, V_{gq} = 0,V_{gd}= V_g, then :

$$P_s(t) = \frac{3}{2}\left(V_g(t)i_d(t)\right) \quad (20)$$

$$Q_s(t) = \frac{3}{2}\left(-V_g(t)i_q(t)\right) \quad (21)$$

2.5.2. Control strategy

The proposed control strategy of the three level NPC inverter and the system power is based on the use of a discreet time integral sliding mode controller (Utkin et al. 1999; Golo and Milosavljevic 2000). This choice is motivated by its robustness against DC sources and grid uncertainties, and also by its capability to eliminate the reaching phase (compared to traditional sliding mode control).

The system given in (17) has the form :

$$\dot{X} = AX + BU + C \quad (22)$$

With:

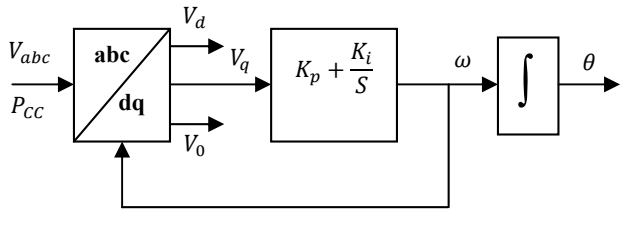

Fig. 4. Schematic diagram of the phase locked loop (PLL)

$$A = \begin{bmatrix} \frac{-R}{L} & \omega & 0 \\ -\omega & \frac{-R}{L} & 0 \\ 0 & 0 & 0 \end{bmatrix}, B = \begin{bmatrix} \frac{1}{L} & 0 & 0 \\ 0 & \frac{1}{L} & 0 \\ 0 & 0 & \frac{1}{C_{eq}} \end{bmatrix}, C = \begin{bmatrix} \frac{-1}{L}V_{gd} \\ \frac{-1}{L}V_{gq} \\ 0 \end{bmatrix}$$

First,let consider three new variables :

$$X_1 = \left(i_d - i_{d\,ref}\right),\ X_2 = \left(i_q - i_{q\,ref}\right),\ X_3 = \left(V_{dc} - V_{dc\,ref}\right)$$

Where : the reference currents $(i_{d\,ref}, i_{q\,ref})$ are related to the active and reactive power references in (*dq*) frame by Rahbarimagham et al. (2015) :

$$\begin{cases} P_{rg} = \frac{1}{2}\left(V_{ref} \times I_{dref}\right) \\ Q_{rg} = \frac{1}{2}\left(V_{ref} \times I_{qref}\right) \end{cases} \text{ so } \begin{cases} I_{dref} = \frac{2\,P_{ref}}{V_{ref}} \\ I_{qref} = \frac{2\,Q_{ref}}{V_{ref}} \end{cases} \quad (23)$$

And $V_{dc\,ref}$: is set by the grid-connected system designer (Sarpturk et al. 1987).

With respect to $X = [X_1, X_2, X_3]^T$, our system can be rewritten : $\dot{X} = AX + BU + D$ (24)

With : $D = C + A\left[i_{dref}, i_{qref}, V_{dc\,ref}\right]^T$

In discreet time the model in equation (24) is :

$$X(k+1) = A_d\,X(k) + B_d\,U(k) + D_d \quad (25)$$

Where : A_d, B_d, D_d are discrete time matrices obtained using a zero-order hold to the system.

The objective of this control is to force the system state to reach in a finite time and to remain in a sliding surface $\sigma(x)$ by defining an adequate control low, so that the state trajectories will fellow $\sigma(x) = 0$ with a controlled and stable dynamic behavior .

This sliding surface is possibly chosen to have both of proportional and integral actions, in discrete time this surface is given by: $\sigma(k) = K_P\,X(k) + K_i T_s \sum_{j=0}^{k} X(j)$ (26)

With :K_p, K_i : are the SMC parameters matrices; and (k = 0,1,2,...)

The adequate choice of K_p, K_i will lead the system have in the sliding surface defined by: $\sigma(k) = 0$ (27)

On the other hand: $\sigma(k+1) = K_P\,X(k+1) + \sum_{j=0}^{k} X(k)$ (28)

So : $\sigma(k+1) = \sigma(k) + K_p\left(X(k+1)\right) + (K_i T_S - K_P)X(k)$ (29)

Taking into account (28) and (29) we can easily verify :

$X(k+1) = (I - K_P^{-1}K_i T_S)\,X(k)$ (30)

Which mean that the system state will depend only on the choice of the controller parameters of K_p and K_i.

The proposed controller has the following form in discrete time:

$$\begin{cases} U(k) = U_{eq}(k) + U_{NL}(k) \\ U_{eq}(k+1) = f(U(k)) \end{cases} \quad (31)$$

The equivalent controls U_{eq}(k) is obtained by subsuming (25) and (29) and solving (27) taking into account the recurrent relation of (24) :

$$X(k) = A_d\,X(k-1) + B_d\,U(k-1) + D_d \quad (32)$$

$$\sigma(k+1) = \left[K_p\,(A_d - I) + K_i T_s\right][A_d\,X(k-1) + B_d\,U(k-1) + D_d] + K_p B_d U_{eq}(k) + \sigma(k) = 0 \quad (33)$$

If (K_pB_d) is an invertible matrix, then:

$$U_{eq}(k) = -\left(K_p B_d\right)^{-1}\left[K_p\,(A_d - I) + K_i T_s\right]\left[A_d\,X(k-1) + B_d\,U_{eq}(k-1) + D_d\right] + K_p D_d + \sigma(k) = 0 \quad (34)$$

The control low in (34) allows the system to remain the sliding surface. However, in order to enhance the robustness of the controller, a nonlinear control is added as follow:

$$U_{NL}(k) = N.sign\left(\sigma(k)\right) \quad (35)$$

Where : N is a matrix with constant non negative elements. Hence, the SMC controller is :

$$U_{eq}(k) = -\left(K_p B_d\right)^{-1}\left[K_p\,(A_d - I) + K_i T_s\right]\left[A_d\,X(k-1) + B_d\,U_{eq}(k-1) + D_d\right] + \sigma(k) + N.sign\left(\sigma(k)\right) = 0 \quad (36)$$

2.5.3. Stability of the proposed integral sliding mode controller

In case of discrete time systems, the Lyapunov condition is given by (Sarpturk et al. 1987; Abidi et al. 2007):

$$\|\sigma(k+1)\| < \|\sigma(k)\| \quad (37)$$

From equation (32), $\|\sigma(k+1)\|$ is:

$$\|\sigma(k+1)\| = \left\|\left[K_p\,(A_d - I) + K_i T_s\right][A_d\,X(k-1) + B_d\,U(k-1) + D_d] + K_p B_d U_{eq}(k) + K_p D_d + \sigma(k)\right\| \quad (38)$$

Using the Minkowski inequality propriety:

$$\|\sigma(k+1)\| \le \|\sigma(k)\| + \left\|\left[K_p\,(A_d - I) + K_i T_s\right][A_d\,X(k-1) + B_d\,U(k-1) + D_d] + K_p B_d U_{eq}(k) + K_p D_d\right\| \quad (39)$$

Then:

$$\|\sigma(k+1)\| \le \|\sigma(k)\| + \left\|K_p B_d U_{eq}(k)\right\| + \left\|\left[K_p\,(A_d - I) + K_i T_s\right][A_d\,X(k-1) + B_d\,U(k-1) + D_d] + K_p D_d\right\| \quad (40)$$

So the condition given in (37) is always satisfied if :

$$\left\|K_p B_d U_{eq}(k)\right\| + \left\|\left[K_p\,(A_d - I) + K_i T_s\right][A_d\,X(k-1) + B_d\,U(k-1) + D_d] + K_p D_d\right\| > 0$$

Furthermore, using Holder's inequality:

$$\left\|K_p B_d U_{eq}(k)\right\| \le \left\|K_p\,B_d\,\right\|.\left\|U_{eq}(k)\right\| \quad (41)$$

$$\left\|K_p\,B_d\,\right\|.\left\|U_{eq}(k)\right\| + \left\|\left[K_p\,(A_d - I) + K_i T_s\right][A_d\,X(k-1) + B_d\,U(k-1) + D_d] + K_p D_d\right\| > 0 \quad (42)$$

If : $\left\|K_p\,B_d\,\right\| > 0$; $\left\|U_{eq}(k)\right\| > 0$, thus the stability condition is verified and $\|\sigma(k+1)\|$ will decrease monotonically and converge to :

$$\|\sigma(k+1)\| = 0 \quad (43)$$

In a finite time any control low in the function (36) will satisfy the system stability by choosing the adequate parameters :K_p, K_i matrices, and due to practical limitations equivalent control can be easily limited:

$$\left\|U_{eq}(k)\right\| < U_{Max} \quad (44)$$

2.5.4. Three-level space vector modulation (SVM)

This section presents the three-level NPC inverter SVM topology, the output voltages can be presented in the space on a ($\alpha\beta$) plane corresponding to the switching states of the inverter. Base on their magnitudes, the 19 space vectors correspond to the 27 switching states of the three-level NPC inverter and the projection of the vectors on a ($\alpha\beta$) coordinates forms a two-layer hexagon centered at the origin of the ($\alpha\beta$) plane. Zero voltage vectors are located at the origin of the plane. The switching states are illustrated by 0, 1 and 2 which denote corresponding switching states (Ramírez et al. 2012; Kartick et al. 2016). The demand vector, $V_{ref,}$ is the geometric sum of the chosen three vectors ($V_{1,}$ $V_{2,}$ V_3) multiplied by their switch on duration ($d_{1,}$ $d_{2,}$ d_3) and sum of their switch on duration must be equal to complete cycle T.

$$\begin{aligned} V_1 d_1 + V_2 d_2 + V_3 d_3 &= V_{ref} T \\ d_1 + d_2 + d_3 &= T \\ V_{ref} = \left|V_{ref}\right| e^{j\theta}\ ;\ \theta &= \angle V_{ref} \end{aligned} \quad (45)$$

3. Power management strategy

In order to prove the effectiveness of the previous strategy, a power management strategy is adopted as follow:

– A reference active and/or reactive power is produced by the hybrid generation system using both of PV and SOFC sources, the objective is to have a fixed stable generated power from the system; this reference can be changed according to the grid demand and independently of the local load demand;

– If the power generated by the PV-FC systems is independent of local load demand, then, the system is functioning in unit-power control mode (UPC mode);

– If the power reference of the PV-FC systems is fixed to be equal to the local load demand, then, the system is functioning in feeder-flow control mode (FFC mode);

–The SOFC acts as a secondary source to ensure a smooth and shaped delivered power to the load and main grid even in poor weather conditions or at night;

– If the local load power demand is less than the reference power generated by PV-FC system, the excess power will be injected to the grid;

– If load demand is more the hybrid system generation capability, the remaining power to supply the load demand will be generated by the grid.

4. Simulation results

To investigate the effectiveness of the proposed control strategy, a complete simulation of the closed loop HES hybrid system including its components modeling, the global control (integral sliding mode control) of the three levels NPC interface inverter

and the local controllers (PI and MPPT) applied to boost converters has been carried out with the parameters given in appendix and PV array parameters given by the following figures (5.a), (5.b):

5. 1. Unit power control (UPC) mode

In this mode, the generated power by HES hybrid system is independent of the load. A step of real power from 150 *KW* to 100 *KW* at *t*=2 *s* with reactive power equal to zero are considered. The weather conditions fixed are supposed to *T*=25° C and irradiance *E*=1000 W/m^2 also we consider a step variation of the load from 100 *KW* to 150 *KW* at *t* =1 *s*. The simulation results are given in figures 6-12.

From the simulation results, the oxygen flow is obtained by dividing the hydrogen flow to oxygen ratio. In the data, the ratio has been taken as 1.145 in the model. The initial oxygen flow rate is 0.239 (Mol/s), the initial value of the hydrogen flow in the SOFC is $q_{H2} = 0.274$(Mol/s), which correspond to the theoretical value obtained by taking the initial current $100\,A$. The number of cells connected in series is taken as 450. For a 50 *K*W, the SOFC output voltage is 403*V*, then it dropped to 0 when *t* >2s, since the PV array will produce a constant power correspond to its optimal functioning conditions P_{pv} = 100.7 *K*W; the SOFC will produce the remaining power of *P*= 49.3 *K*W when *t*<2 s. If the load need less than the power generated by the hybrid system (which is the case when *t*<1 s), the extra power will be injected to the grid. If more power is needed by the load or one of the hybrid system components is in fault condition; the extra power will produced by the grid which is the case when *t* >2 *s*. The reactive power reference is also controlled independent of the load, if it is set to zero, the needed load reactive (*Q*=1000 *VAR*) power will be produced by the grid.

The steady state error between the reference power and the power generated by the PV system is practically null which validate the good performances of the discrete time integral SMC controller behavior under fixed reference.

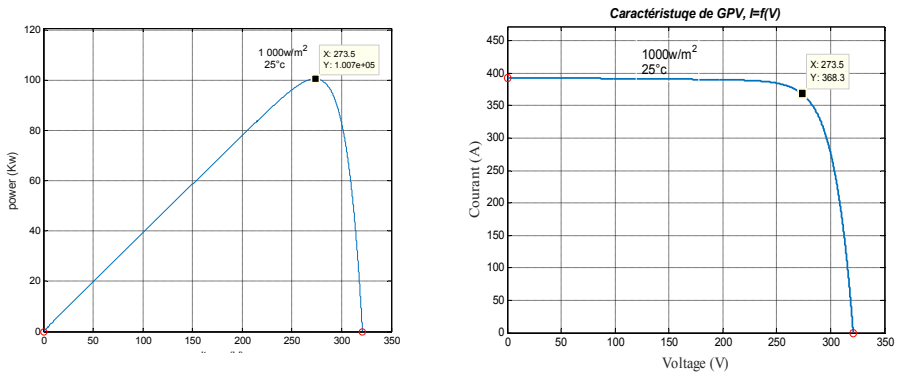

Fig. 5. (a) Photovoltaic array power *P*=*f*(*V*) and (b) Current photovoltaic array power *I*=*f*(*V*).

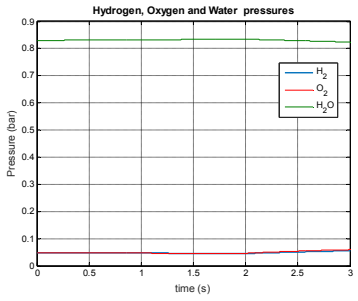

Fig. 6. Hydrogen, Oxygen and water pressures

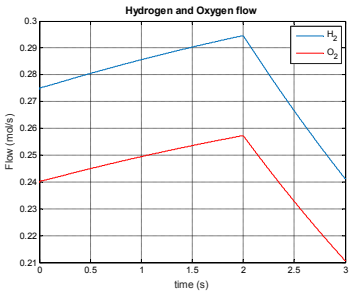

Fig. 7. Hydrogen, Oxygen flow

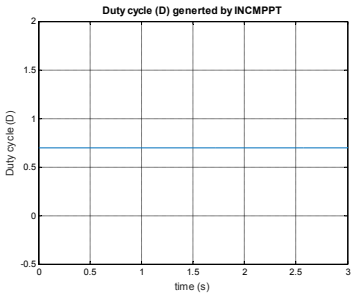

Fig. 8. Duty cycle (D) generated by INCMPPT

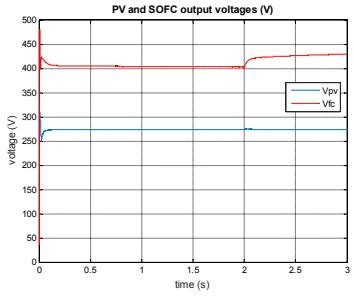

Fig. 9. PV and SOFC output voltages (*V*)

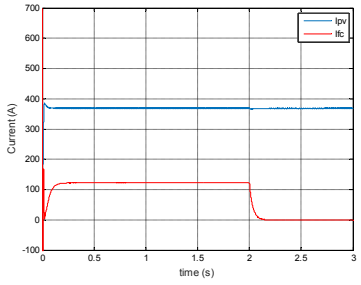

Fig. 10. PV and SOFC output currents (*A*)

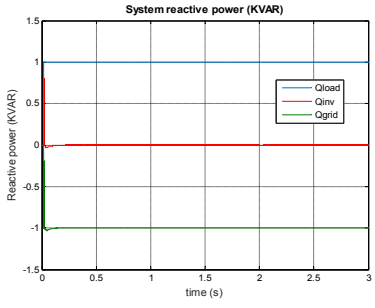

Fig. 11. System reactive power (*KVAR*)

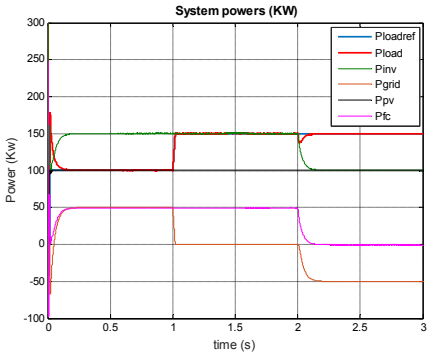

Fig. 12. System powers (*KW*)

5.2. Feeder flow control (FFC) mode

In this mode the same HES hybrid system it tested under a variable load, the amount of the power generated is related directly to its local load, For simulation purposes, let consider first that the PV array is producing a fixed amount of power by considering a fixed whether condition. With the same weather conditions (T=25° C and E=1000 W/m^2), the results are given in figures 13-18.

The power production is depending on load condition, the hybrid system adjust its power reference in real time to meet the local load need. The SOFC assists incapable to satisfy the load need in steady state by adjusting its production according to that are due to PV array generation transients. The main grid contribution to the local power flow is limited only in case of fast load change (step variation) due to time constant of the SOFC, or when the PV-FC system maximum production limit is reached. The remaining power to supply the load will be produced by the main grid (e.g., t>2s in systems active powers simulation results) which eliminate the need of a storage device in this system.

Nevertheless, in islanded mode (standalone mode) a more fast and high density storage device like a super-capacitor is needed to enhance the dynamical response of the system. It can be seen also that for a constant reactive power of the load, this power is produced now by the hybrid system in steady state and the grid will contribute to reactive power generation in transient state. From a control point of view, again, the load and input power variation, has a practically a negligible effect on the system performances, the system has a fast dynamic response (response time tr = 0.1s) with a zero steady state error. In addition, the dc bus voltage is maintained a constant level of value 900 V. The two input capacitors of the three level NPC inverter have practically the half of the dc bus voltage. The FFT analysis of (Line –Line) grid voltage and (Line- Neutral) voltage prove the quality of the output voltage of the system when using SVPWM with discrete integral SMC.

6. Conclusion

This paper presents power management of HES and an effective control strategy under nonlinear load conditions in grid connection. This sliding mode control is proposed for two operating modes and power management of the overall system (UPC and FFC modes), high performances have proven in the two operating cases. The proposed fixed frequency sliding mode control is formulated in (*dq*) reference frame taking into account that the dc voltage stability is ensured first by the localized control of each dc source separately, then, by sliding mode control which ensure also the power regulation. The results show that an improved power quality is guaranteed using NPC multi levels inverters even under nonlinear load conditions.

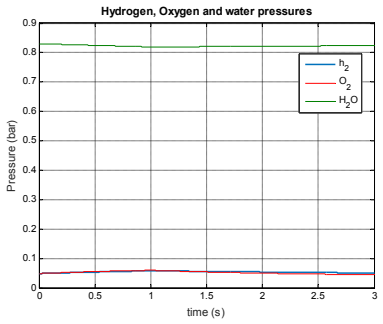

Fig. 13. Hydrogen, Oxygen and water pressures

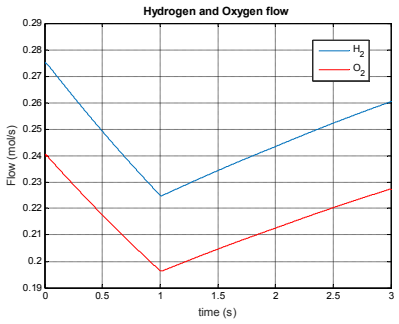

Fig. 14. Hydrogen, Oxygen flow

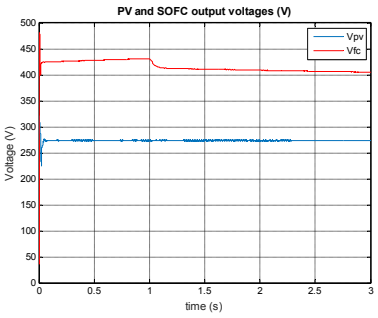

Fig. 15. PV and SOFC output voltages (*V*)

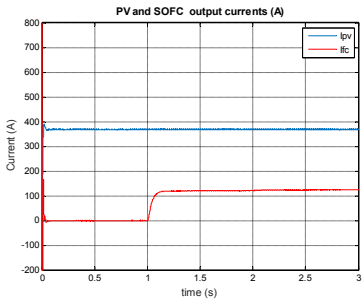

Fig. 16. PV and SOFC output currents (*A*)

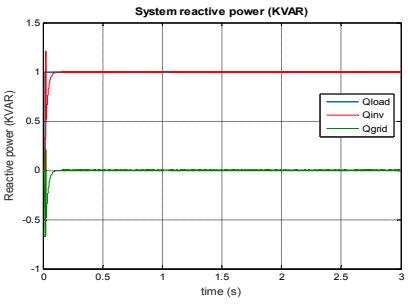

Fig. 17. System reactive power (*KVAR*)

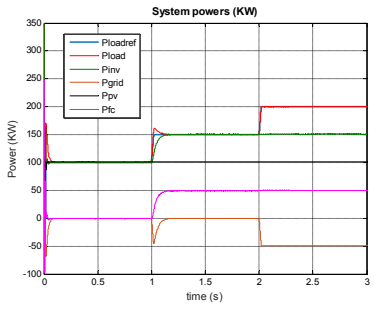

Fig. 18. System powers (*KW*)

Appendix

A. Parameters values of photovoltaic array (at 25^{0}C) are given as bellow

Numbers of the series modules = 5; Numbers of the parallel modules = 66
Numbers of the cells per module = 96; Open circuit voltage Voc = 64.2 *V*
Short-circuit current *Isc* = 5.96 *A;* Voltage at max. power point V_{mp}=54.7 *V*
Current at maximum power point Imp = 5.58 *A;* Diode Quality factor=1.25
Photo-current source I_{ph}=5.96 *A;* Diode saturation current Isat=5.26.10^{-9} *A*
Parallel resistance R_p = 819.13 Ω; Series resistance R_s = 0.083 Ω

B. Parameters of DC-DC Boost converter (connected to PV)

Switching: *f*s=5.4 *Khz, L*= 4 *mH*; r_l=0.01 Ω;*C*= 2000 μF, r_c=0.01 Ω

C. Parameters of DC-DC Boost converter (connected to SOFC)

Switching : *f*s=5.4 Khz, *L*= 5 *mH*; r_l=0.01 Ω;*C*= 5000 μF, r_c=0.1 Ω

D. Solid Oxide Fuel (SOFC) parameters

Var.	Representation	Value
T	Absolute temperature	1273 *K*
F	Faraday's constant	96487 *C/mol*
R	Universal gas constant	8314 (*J/ Kmol K*)
E_0	Standard reversible cell potential	1.18 *V*
N	Number of cells in stack	450
K_r	Constant	996*10^{-6} (*Kmol/sA*)
U_{max}	Maximum fuel utilization	0.9
U_{min}	Minimum fuel utilization	0.8
U_{opt}	Optimum fuel ratio	0.85
K_{H2}	Value molar constant for hydrogen	8.43*10^{-4} *Kmol//(s atm*)
KO_2	Value molar constant for oxygen	2.81*10^{-4} *Kmol//(s atm*)
KH_2O	Value molar constant for water	2.52*10^{-3} *Kmol//(s atm)*
τ_{H2}	Response time for hydrogen flow	26.1 s
τ_{H2O}	Response time for water flow	78.3 *s*
τ_{O2}	Response time for oxygen flow	2.91 *s*
R	Ohmic loss	0.126 Ω
T_e	Electric response time	0.8 *s*
T_f	Fuel processor response time	0.03 *s*
r_{HO}	Ration of hydrogen to oxygen	1.145

E. Inverter and Grid parameters

Rated power *P* =200 *KW* ; Frequency *f*s=5.4 *Khz*
Voltage amplitude (line-line r_{ms} value) $V_{L\text{-}L}$=400 *V*
Output filter: L_f=3.5.10^{-3} *H*
Grid resistance *R*g=0.012 Ω
Voltage ampl. (line-neutral r_{ms} value) V_{ln}=230 *V*
Equivalent Input capacitor Ceq=6000 μF
Grid inductance Lg=3.10-4 *H*
DC voltage (reference) = 900 *V*
(450 *V* in each capacitor in balanced conditions)

F. Controllers parameters

(DC-DC) Boost converter PI controller: *k*p =0.001, *k*i =0.15
Discreet time integral sliding mode controller:

$$K_p = \begin{bmatrix} 0.7 & 0 & 0 \\ 0 & 0.7 & 0 \\ 0 & 0 & 2 \end{bmatrix}, K_i = \begin{bmatrix} 6.10^3 & 0 & 0 \\ 0 & 6.10^3 & 0 \\ 0 & 0 & 35.10^2 \end{bmatrix}; N = \begin{bmatrix} 0.015 & 0 & 0 \\ 0 & 0.015 & 0 \\ 0 & 0 & 0.01 \end{bmatrix}$$

References

Abidi, K., J.X Xu, Y. Xinghuo (2007) On the discrete-time integral sliding mode control, Transaction on Automatic Control 52(4): 709-715.

Benghanem, M., A. Drao (2006) A new modelling and control analysis of an advanced static var compensator using a three-level (NPC) inverter topology. Journal of electrical engineering 57(5): 285-290.

Bieberle, A., L.J. Gauckler (2002) State-space modeling of the anodic SOFC system N_i, H_2–H_2O–YSZ," Solid state ionics journal 146 (1-2): 23-41.

Bouafia, S., A. Benaissa, M. Bouzidi, S. Barkat (2014) Sliding mode control of three levels back-to-back VSC HVDC system using space vector modulation system using space vector modulation. International Journal of Power Electronics and Drive System (IJPEDS) 4(2): 265-273.

Erickson, R.W., D. Maksimovic (2001) Fundamentals of power electronics, Second edition, Kluwer Academic Publishers, New York.

Golo, G., C. Milosavljevic (2000) Robust discrete-time chattering free sliding mode control, Systems and control letters 41(1): 19-28.

Hazem, O.M., Y. Amirat, M. Benbouzid, A. Elbaset (2014) Optimal design of a pv/fuel cell hybrid power system for the city of Brest in France, IEEE ICGE 2014, Mar 2014, Sfax, Tunisia. pp. 119-123.

Kartick J.C., B.K. Sujit, K.C. Suparna (2016) Dual reference phase shifted pulse width modulation technique for a N-level inverter based grid connected solar photovoltaic system, in IET Renewable Power Generation 10(7): 928-935.

Khanh, L.N., J.J. Seo, Y.S. Kim, D.L. Won (2010) Power-management strategies for a grid-connected PV-FC hybrid system. IEEE transactions on power delivery 25(3): 1874-1882.

Larminie, J., A. Dicks (2003) Fuel Cell Systems Explained, 2nd edition. New York: Wiley.

Lasseter, R.H. (2011) Smart distribution: coupled microgrids Proceedings of the IEEE 99 (6): 1074-1082.

Lopes, J.A.P., C.L. Moreira, A.G. Madureira (2006) Defining control strategies for microgrids islanded operation IEEE Transactions on power systems 21 (2): 916-924.

Paolo, P., R.H. Lasseter (2006) Autonomous control of microgrids. IEEE PES Meeting, Montreal, 1-8.

Portillo, R., S. Vazquez, J.I. Leon, M.M. Prats, L.G. Franquelo (2013) Model based adaptive direct power control for three-level npc converters, IEEE Transactions on industrial informatics 9(2): 1148-1157.

Rahbarimagham, H., E.M. Amiri, B. Vahidi, G. Gharepetian, M. Abedi (2015) Superior decoupled control of active and reactive power for three-phase voltage source converters. Turkish Journal of Electrical Engineering & Computer Sciences 23(4): 1025-1039.

Ramírez, J. D.B., J.R. Rivas (2012) DSP-based simplified space-vector pwm for a three-level vsi with experimental validation, Journal of power electronics 12(2): 285-293.

Sarpturk, S.Z., Y. Istefanopulos, O. Kaynak (1987) On the stability of discrete-time sliding mode control systems, IEEE Transaction on Automatic Control 32(10): 930-932.

Sezen, S., E. Özdemir (2013) Modeling, simulation and control of three-phase three level multilevel inverter for grid connected photovoltaic system, Journal of optoelectronics and advanced materials 15(3-4): 335-341.

Utkin, V., J. Gulder, J. Shi (1999) sliding mode control in electro-mechanical systems, Taylor and Francis, London, U.K.

Villalva, M. G., J.R. Gazoli, E.R. Filho (2009) Comprehensive approach to modeling and simulation of photovoltaic arrays, IEEE Transactions on power electronics 24 (5): 1198-1208.

Zhang, X., J.W. Spencer, J.M. Guerrero (2013) Small-signal modeling of digitally controlled grid-connected inverters with lcl filters, IEEE Transactions on industrial electronics 60(9): 3752-3765.